In situ monitoring and analysis of enamel demineralisation using synchrotron X-ray scattering

Sui, Tan; Salvati, Enrico; Harper, Robert; Zhang, Hongjia; Shelton, Richard; Landini, Gabriel; Korsunsky, Alexander M.

[Link to publication on Research at Birmingham portal](#)

In situ monitoring and analysis of enamel demineralisation using synchrotron X-ray scattering

Tan Sui[1,3*], Enrico Salvati[1], Robert A. Harper[2], Hongjia Zhang[1], Richard M. Shelton[2], Gabriel Landini[2], Alexander M. Korsunsky[1*]

[1] Department of Engineering Science, University of Oxford, Parks Road, Oxford, OX1 3PJ, U.K.

[2] School of Dentistry, College of Medical and Dental Sciences, University of Birmingham, 5 Mill Pool Way, Edgbaston, Birmingham, B5 7EG, U.K.

[3] Department of Mechanical Engineering Sciences, University of Surrey, Guildford, Surrey, GU2 7XH, U.K.

* Corresponding authors: t.sui@surrey.ac.uk; alexander.korsunsky@eng.ox.ac.uk

Abstract

Dental caries is one of the most common chronic diseases that affect human teeth. It often initiates in enamel, undermining its mechanical function and structural integrity. Little is known about the enamel demineralisation process caused by dental caries in terms of the microstructural changes and crystallography of the inorganic mineral phase. To improve the understanding of the carious lesion formation process and to help identify efficient treatments, the evolution of the microstructure at the nano-scale in an artificially induced enamel erosion region was probed using advanced synchrotron small-angle and wide-angle X-ray scattering (SAXS and WAXS). This is the first *in vitro* and time-resolved investigation of enamel demineralisation using synchrotron X-ray techniques which allows *in situ* quantification of the microstructure evolution over time in a simulated carious lesion. The analysis revealed that alongside the reduction of mineral volume, a heterogeneous evolution of hydroxyapatite (HAp) crystallites (in terms of size, preferred orientation and degree of alignment) could be observed. It was also found that the rate and direction of dissolution depends on the crystallographic orientation. Based on these findings, a novel conceptual view of the process is put

forward that describes the key structural parameters in establishing high fidelity ultrastructure-based numerical models for the simulation of the enamel demineralisation process.

Keywords: Dental caries, dental demineralisation; Enamel; SAXS; WAXS; *in situ* analysis

Significance

Hydroxyapatite (HAp) crystallites in the enamel dissolve during dental caries although little is known about the structural-chemical relationships that control the dynamic demineralisation process. For the first time this work investigated the *in situ* evolution of nano-scale morphology and the spatial distribution of HAp crystallites in human enamel during demineralisation in simulated caries. Advanced synchrotron SAXS and WAXS techniques showed that the heterogeneous evolution of crystallites (size, preferred orientation and degree of alignment) could be attributed to a crystallographic-orientation-dependent anisotropic dissolution. Hence we propose a novel conceptual scheme to describe the demineralisation process. These findings appear to have important implications for understanding the detailed mechanisms of enamel demineralisation and provide insight into potential enamel remineralisation that could restore structural integrity and function.

Graphical Abstract
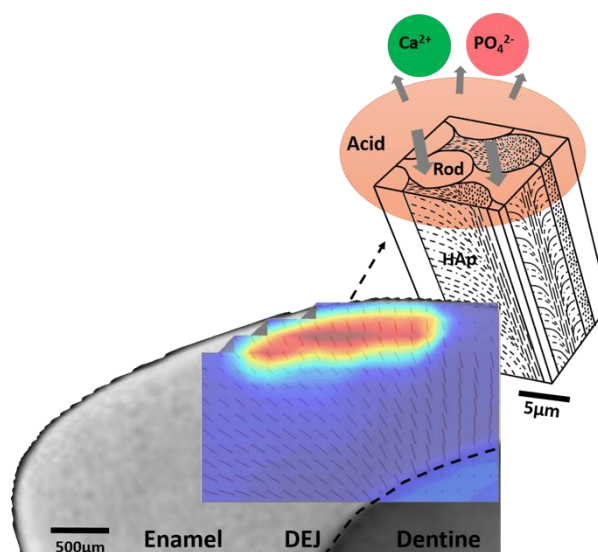
1. Introduction

Enamel is a highly mineralised and extremely hard tissue (96% inorganic content by weight) that covers the crown of teeth. The resistance to masticatory forces, thermal shocks and acids is conferred on the enamel by its intricate hierarchical two-level composite structure. The microstructural level is represented by a rod and inter-rod structure which in cross sections exhibits a keyhole-like appearance and the nano-scale by the organized and bundled needle-like hydroxyapatite (HAp) crystallites within each rod/inter-rod with the formula $Ca_{10}(PO_4)_6OH_2$. Owing to a greater organic component, crystallites in the inter-rod areas have a less aligned distribution than those in the rod areas [1, 2]. The length of the HAp crystallites has been reported to be from several tens of nanometres (40-50nm) [3] to even the entire thickness of the enamel layer [4]. Extraneous ions such as carbonate, fluoride, sodium and magnesium are often found to precipitate within the crystal structure [5].

Enamel caries is a form of enamel destruction by demineralisation caused by acids (predominantly lactic acid) produced by cariogenic bacteria in dental plaque when anaerobically metabolising certain type of carbohydrates in the diet [6]. The enamel demineralisation *i.e.* diffusion of acid into enamel crystallites, depends on factors such as acid type, pH value of the solution [7], acid concentration, acid titration, and the duration of acid exposure [8]. Structural-chemical changes occurring in a low pH environment destroy the enamel surface by partial or complete dissolution of the HAp crystallites, resulting in the release of Ca^{2+} and HPO_4^{2-} ions, the loosening of the micro-/nano-structure of enamel, which in turn causes a loss of mechanical function, resulting in inaesthetic appearance and potentially leading to pain if the lesion extends into dentine. In natural early enamel carious lesions (i.e. with no evident cavity formation and clinically visible as 'white spots'), four zones can be defined in bright filed microscopy sections. From the surface to the enamel depth these are the surface zone, the body of the lesion, the dark zone and the translucent zone [9]. *In vitro* artificial caries-like lesions can be generated by acidic buffers (for example, acetic acid or lactic acid

[10]). However, these may not necessarily produce the zones mentioned earlier, and could generate a steady gradient of dissolution from the enamel surface towards the bulk of the enamel [11].

Considerable efforts have been directed towards the study of natural and artificial carious lesions *ex situ* using conventional and advanced techniques, such as quantitative light-induced fluorescence [12], atomic force microscopy [13] and secondary ion mass spectroscopy (SIMS) [14]. Synchrotron X-ray scattering techniques have been well established for spatially resolved 2D characterisation and quantification of dental tissue structures across the length scale. For example, small-angle X-ray scattering (SAXS) has been applied to investigate the structural changes, e.g. enamel pore formation [15] and preservation of the dentine collagen network [16] of carious lesions at the nano-scale, while wide-angle X-ray scattering (WAXS) has been applied to characterise the crystallographic texture of HAp crystallites as well as the loss of the mineral mass in natural and artificial carious lesions [17, 18].

These observations have demonstrated important and characteristic changes in the structure of enamel caries, e.g. pore formation and crystallographic texture, however, *ex situ* experiments are snapshots of a process and hence provide incomplete information of the enamel caries progression. Few attempts have been made to study enamel demineralisation using *in situ* methodologies [19, 20]. Most studies have been limited to the observation of mineral weight loss, without detailed spatial resolution or probing for underlying structural changes. Critical insights into the nature and time-resolved evolution of the chemical reactions taking place during enamel demineralisation and the consequent micro- and nano-structural changes are therefore still lacking. To the authors' best knowledge, the present study is the first investigation of enamel demineralisation using synchrotron X-ray techniques that provides an insight into the evolution of the ultrastructural changes with time, and suggests a preliminary model to describe enamel demineralisation.

The motivation for this study was therefore to facilitate the quantitative analysis of the main parameters of the chemical reactions involved (e.g. acid front and dissolution rate) by *in situ* multi-

scale characterisation of artificially induced enamel demineralisation. The synchrotron-based experimental approach combined two powerful X-ray scattering techniques (SAXS/WAXS) to provide a deeper insight into the structural changes at different length scales that occurred during enamel demineralisation, aiming to identify the necessary parameters for developing ultrastructure-based models simulating structural evolution and its consequences (e.g. mechanical response) to help pave the way towards a more fundamental understanding of the caries disease process and any long-term solution that could be developed.

2. Materials and methods

2.1 Sample preparation

A freshly extracted human third molar with no apparent damage, caries or other dental treatments was used for this study (ethical approval obtained from the National Research Ethics Committee; NHS-REC reference 09.H0405.33/ Consortium Reference BCHCDent332.1531.TB). Slices containing both dentine and enamel were cut to a thickness of 200μm using a low speed rotating diamond saw (Isomet, Buehler, UK). Samples were stored in phosphate-buffered saline (PBS) until the synchrotron experiment was performed.

2.2 *In situ* scattering measurements

2.2.1 Enamel demineralisation setup

In this study, lactic acid was chosen as the erosion inducing agent because it is a prominent product of cariogenic plaque linked to dental caries [6]. A 10% v/v lactic acid (pH 2.2, 100μL) solution was selected to simulate carious acid dissolution in Sample #1 to obtain a reasonable timescale for the synchrotron experiment. To monitor enamel demineralisation, the sectioned surfaces of the tooth slice were firstly covered with commercial nail varnish spiked with methylene blue dye powder (to aid visualisation), leaving only a single uncovered margin of enamel as a free

5

surface. Application of varnish had minimal influence on the scattering patterns generated by the human dental tissues when examined using X-ray scattering. Two pieces of Kapton sheets (DuPont™, USA) were then applied on the vanished surfaces, allowing a small funnel to be made with dental ribbon wax to contain the lactic acid. Dental ribbon wax was then applied to seal the opening between the sheets to prevent acid evaporation. Two tungsten rods were attached on the Kapton sheets using cyanoacrylate cement (Loctite®) and placed on a sample holder for further synchrotron examination.

An attempt was made to assess the demineralisation of enamel using Sample #2 with 2% lactic acid (pH 2.2, 100μL) for 42.5h. However, this 5-fold reduction in acid concentration resulted in a considerably slower and smaller lesion formation for which the analysis beam size of 150μm would not have a resolution sufficient to generate reliable quantitative data (see Supplementary Material Figure S1). In spite of this undesirable outcome, qualitative data was collected showing the enamel dissolution was also induced in that experimental condition.

2.2.2 SAXS/WAXS setup

The experiment was performed at the B16 beamline at Diamond Light source (DLS, UK) using a monochromatic beam energy of 18keV defined by double-crystal Si (111) and spot size of 150μm ×150μm. The region of interest (ROI) was firstly identified as 2.85mm×2.25mm with slits wide open using a sCMOS camera (Photonic Science Ltd. UK). The sample was repeatedly shifted in the *x-y* plane (see Fig. 2) to collect SAXS or WAXS maps. The spacing between each two measurement points was 150μm in both *x*- and *y*-axes, resulting in a total of 285 scattering patterns per map. The initial state of the dental enamel without acid exposure was examined by a SAXS map and the patterns were collected with a sample-to-detector distance of 6510mm with a Pilatus 300K detector (Dectris, Baden, Switzerland) and calibrated using dry chicken collagen as a non-crystalline diffraction standard [21]. WAXS patterns were then collected at a sample-to-detector distance of

110.320mm with an Image Star 9000 detector (Photonic Science Ltd., UK), calibrated using compacted disks of standard silicon powder (NIST SRM640d). Once the preliminary SAXS and WAXS maps were completed, lactic acid was injected into the funnel constructed on the free enamel surface. Loops of SAXS maps followed by the WAXS maps were programmed using a script to run continuously for ~40h. 13 maps of SAXS/WAXS were acquired, one every 3h. The dose has been calculated as 63.35Gv, due to the relatively low flux in the bending magnets beamline. Therefore, the irradiation effect could be neglected.

<<Fig. 1>>

2.3 SAXS/WAXS data interpretation

2.3.1 SAXS data interpretation

The quantitative interpretation of SAXS data provides information of scattering objects at their nano-scale domains, *e.g.* smallest crystalline dimension, orientation and degree of alignment of the nano-crystallites. 2D SAXS patterns (arising from the electron density contrast at the nano-scale) were pre-processed and converted into 1D intensity profiles, which in this study indicated the nano-scale changes occurring at the scattering objects over the acid induced demineralisation. The preferred orientation (ϕ_0) with the degree of alignment (ρ) and smallest crystalline dimension (T) of the HAp crystallites were determined from 1D profiles.

To quantify the spatial arrangement of HAp crystallites (ϕ_0 and ρ) in the *x-y* plane of the sample, the 2D SAXS patterns were processed by integrating scattering vector (q), resulting in a 1D profile of $I(\phi)$, where ϕ_0 was determined by the two peak positions of $I(\phi)$. ρ was calculated by the ratio of the peak areas of $I(\phi)$ to the overall intensity [22, 23]. To quantify the smallest crystalline dimension, the 2D SAXS patterns were processed by integrating the azimuthal angle (ϕ), resulting in $I(q)$ vs. q plot (see Supplementary Material Figure S2 (a)) [24-26]. *T* is defined as the *Porod* chord length based on *Porod's law*, valid in a two-phase system, which represents the total surface area of the

7

particles per unit volume, i.e. the average thickness: $T=(4/\pi)(Q/P)$, where Q is the integrated area of the $I(q){\times}q^2$ vs. q plot (see Supplementary Material Figure S2 (b)) at q range (0.019769nm^{-1}- 0.141278nm^{-1}). P is the *Porod* constant given by $I(q)=P/q^4 + $ B, where P and the constant background B can be determined from $I(q){\times}q^4$ vs. q^4 plot (see Supplementary Material Figure S2 (c)) at large q range (0.141278nm^{-1}- 0.184474nm^{-1}). Note that the volume fraction is not considered in the smallest crystalline dimension calculation as it changes during the demineralisation process. The data analysis was conducted in accordance with previous studies on human dentine and enamel using synchrotron SAXS and WAXS techniques [27-29].

2.3.2 WAXS data interpretation

Quantitative analysis of WAXS data gives insights into characteristic information related to the crystalline structure, e.g. the amount, d spacing between the lattice planes and size of crystals in the gauged volume. Similar to the pre-processing of 2D SAXS patterns, the 2D WAXS patterns were firstly converted into 1D intensity profiles for further interpretation, however the interpretation of the 1D profiles follows *Bragg's* law, which was different from the SAXS data interpretation. The (002) Bragg peak, which represents the orientation of the scattering vector along the hexagonal c-axis of HAp crystallites (CIF file 1011242), has been frequently chosen for the analysis of human dental tissues, as the overall diffraction from the (002) family of lattice planes is the most distinct [30, 31]. In this work, the intensity of the (002) peak (I_{002}) was extracted and the peak centre position was analysed to reveal the spatial variation of the d_{002}-spacing and its evolution over time. The width of the (002) peak was used to determine the crystalline length L by applying the *Scherrer* equation: $L = \dfrac{k\lambda}{Bcos\theta}$, where k is a constant close to unity, λ is wavelength, B is full width at half maximum (FWHM) of (002) peak and θ is the half scattering angle of the (002) peak [32].

3. Results

The snapshots of 2D mappings of SAXS/WAXS results of Sample #1 at different stages of reaction provided a general qualitative understanding of the spatial variation and evolution of the underlying structure to the acid exposure. A line profile from column 9 of each 2D map of sample #1 was selected to illustrate detailed quantitative information of SAXS total intensity over the whole q range, WAXS (002) peak intensity, average nano-crystalline length and thickness, preferred orientation and degree of alignment of HAp crystallites. Column 9 is a representative line that covers the acid contact surface into the unaffected regions of the enamel and no dependency of the measurement results on the line position was found. This typically covered a region from the free enamel surface in contact with the acid down to the base of the sample (dentine). In addition, the chemical dissolution rate was quantified by comparing the 1D profile at 3h and 36h. The initial state (0h) was not used as there were likely small movements of the sample during the addition of the acid.

3.1 SAXS

3.1.1 SAXS total intensity

The 2D mapping of SAXS total intensity profiles after 3, 18 and 36h are shown in Figure 2a. The SAXS total intensity was found to be quite uniform throughout the sample during the early stages (3h) and became increasingly prominent around the contact region during later stages (18 and 36h), as depicted by the yellow to red areas in Figure 2. SAXS pattern intensity depends on the difference of the electron density between the intact HAp crystallites and the surrounding media. The enhanced intensity apparently revealed that the acid attack increased the electron density contrast [33]. As the q range has covered features from ~34nm to ~318nm, which could have been well above the putative pore size, the surrounding media could have contained dissolved crystallites as well as the increased number of pores.

The 1D spatial variation of the SAXS total intensity across the sample (column 9, marked by a white dashed line in Figure 2a) and its evolution with respect to the reaction time is illustrated in

Figure 2b. The 0µm location was at the free enamel surface, where the enamel contacted the acid. An increasingly pronounced peak with time can be seen at around 200 to 400µm enamel depth. Note that the peak centre shifts from ~200µm into the deeper bulk up to ~300µm, indicating the advance of the dissolution front into the depth of the enamel. The deepest regions appeared to remain relatively unaffected after 36h of acid exposure. Figure 2c plots the SAXS total intensity at the first (3h) and last stage (36h) to provide a clear comparison of the intensity difference before and after acid contact. The peak centre positions were quantified by Gaussian function fitting and were found to be 150µm for Sample #1 at 3h, and 315µm for Sample #1 at 36h. The dissolution rate was then calculated from the peak centre position shift rate, which was 5µm/h for 10% lactic acid (100µL) at this pH value (2.2).

<<Fig. 2>>

3.1.2 HAp smallest crystalline dimension

The 2D maps in Figure 3a show the spatial distribution of the smallest crystalline dimension of the nano-domain structures, *i.e.* the HAp crystallites in enamel. Initially the smallest crystalline dimension was larger (>20nm) close to the free enamel surface (dark red area in Figure 3a) and decreased towards the dentine-enamel junction (DEJ, as shown in black dashed lines in Figures 1-7) (~10nm). The layer containing HAp crystallites with the smallest crystalline dimension gradually disappeared after exposure to acid, as a result of crystallite demineralisation. This process appeared to be very rapid at the early stage, compared with the intensity variation shown in Figure 2a, while no significant changes could be observed between 18h and 36h. Such a trend was also seen in the 1D profile along the black dashed line (same position as the white dashed line in Figure 2a) shown in Figure 3b. A dramatic decrease of the smallest crystalline dimension occurred only during the first 6h of acid exposure which stabilised after 6h. Similar to Figure 2c, the difference between the smallest crystalline dimension of HAp in Sample #1 at 3h and 36h is shown in Figure 3c. Apart from

10

the significant drop of the smallest crystalline dimension (~25%) at ~300μm enamel depth, another interesting feature was that the smallest crystalline dimension increased ~600μm away from the enamel free surface.

<<Fig. 3>>

3.1.3 HAp crystalline orientation and degree of alignment

Figure 4a presents 2D maps of the spatial variation of the crystalline orientation (represented by the vector direction), the in-plane degree of alignment (represented by the vector length) and their evolution with time of acid exposure. Crystallites with pronounced degrees of alignment were observed to orient roughly perpendicular to the DEJ. To elucidate the demineralisation process, the results at 3h, 18h and 36h are also shown in Figure 4a. Note that the initial low degree of alignment close to the enamel free surface (see the map at 3h) appeared to gradually increase with the time of acid exposure, *i.e.* the HAp crystallites gradually became aligned.

1D profiles of the evolution of the degree of alignment (length of the vectors in Figure 4a) at column 9 are presented in Figure 4b. In contrast with the rapid change of the smallest crystalline dimension shown in Figure 3b, the degree of alignment indicated a slower evolution with time. The 1D profiles at 3h and 36h are compared in Figure 4c. A significant increase in the degree of alignment could be seen at ~200μm enamel depth while a decrease in the degree of alignment was observed between 400-700μm depth. Note that Figure 3c showed the smallest crystalline dimension increased at ~200-400μm enamel depth, but decreased at ~500-800μm enamel depth.

<<Fig. 4>>

3.2 WAXS

3.2.1 WAXS (002) peak intensity

2D maps of WAXS (002) peak intensity at different stages are shown in Figure 5a, but no clear trend could be seen, except that the width of the peak intensity (dark red area) appeared to gradually shrink. This was confirmed in the 1D intensity profile plot (Figure 5b) along the black dashed line in Figure 5a, where only minor decreases at different times were observed. Figure 5c compares the results at 3h and 36h, showing a visible peak narrowing with a drop of intensity from the free enamel surface to ~600-800µm enamel depth. The weakened intensity revealed that the acid exposure decreased the volume of HAp crystallites during the demineralisation.

<<Fig. 5>>

3.2.2 HAp crystallites d_{002}-spacing

Figure 6a depicts the 2D maps of the spatial variation of the d_{002}-spacing of the crystallites and their evolution with time. In the 2D maps, the d_{002}-spacing gradually decreased with time close to the free enamel surface, but increased to the deeper enamel, which is confirmed in the 1D profile plots in Figure 6b. The gradual reduction of d_{002}-spacing close to the free enamel surface of the sample up to ~200µm enamel depth was likely to be associated with the lattice defects or disorder due to the chemical attack [34].

<<Fig. 6>>

3.2.3 HAp crystalline length

Figure 7a illustrates the 2D map of the spatial distribution of the HAp crystalline length and its evolution with time. A decrease of the crystalline length with time was observed, in particular at the region close to the free enamel surface. The trend in the 1D profile plots shown in Figures 7b and c is similar to that in Figure 6b and c, where the decrease of the HAp crystalline length only occurred close to the free enamel surface, up to ~200µm depth. Note that such decrease in the characteristic

length may be further correlated with the reduction of the smallest crystalline dimension as revealed in Figure 3, at the same regions.

<<Fig. 7>>

4. Discussion

In this work, both SAXS and WAXS measurements have provided a number of indicators that reflect the mineral loss in the artificially induced enamel demineralisation process. From SAXS observations, both the degree and rate of mineral demineralisation can be qualitatively traced by the change of the peak intensity value and the peak centre position in SAXS total intensity profiles (Figure 2). However, the heterogeneous change in preferred orientation shown in Figure 4 seemed to show the crystalline orientation-dependent demineralisation process, with more severe changes occurring just beneath the free enamel surface (Figure 4a). This indicated that this method reliably mimicked *in vivo* conditions, which allowed a subsurface lesion to form similar to those observed in natural enamel carious lesions [18]. In addition, the demineralisation process in our study appeared to be quite non-linear (both in time-scale and also depth-direction), compared with the close-to-linear mineral loss of enamel demineralisation with time along the dissolution direction shown by Cheng *et al* [13]. Such a dynamic process would not be revealed by *ex situ* scanning of the lesions. Once the dynamic process reaches an equilibrium state, the overall orientation and anisotropy of the SAXS signal would remain unaltered throughout the lesion, as previously observed in natural carious lesions [15]. Note that the natural carious lesions in that study showed no visible orientation changes [15], perhaps because 3D diffusion occurred in the complex oral environment. One hypothesis for the observed trend was that the anisotropic dissolution depended on the contact surface area between the crystallites and the acid as it travels from surface to depth. Crystallites perpendicular to the dissolution direction would dissolve faster, eventually leaving crystallites with preferable orientation along the dissolution direction. As a consequence, determination of the actual dissolution rate must

13

depend on the crystalline orientation. Furthermore, another feature, the smallest crystalline dimension, appeared to show the opposite trend to the degree of alignment (Figure 3&4). Near the enamel free surface, crystallites with orientation other than the preferred orientation were dissolved by the acid, resulting in the decrease in the smallest crystalline dimension (Figure 3) and an increase in the degree of alignment (Figure 4). However, in the deeper enamel, re-precipitation of the dissolved calcium and phosphate is possible to have occurred following a process called 'remineralisation' when the environmental pH gradually recovered [35, 36], consequentially increasing the smallest crystalline dimension but decreasing the degree of alignment. The exhibited gradual evolution of the degree of alignment throughout the period compared with the rapid change of the smallest crystalline dimension (Figures 3b &4b) may be an indication that the changes of degree of alignment is more sensitive to remineralisation.

From the WAXS observations, firstly, crystalline length (Figure 7) seemed to show that the highest mineral loss occurred at the free enamel surface. This was also the conclusion drawn from the *ex situ* observations of artificially demineralised enamel, where a decrease in mineral mass (~10%) was observed at the free surface, which was the direct site of acid attack [17]. However, the enamel surface to ~ 600μm was structurally impaired as the WAXS (002) peak intensity (Figure 5) demonstrated a significant uniform mineral loss from the free enamel surface to the deeper enamel (~600μm). In contrast, a small spatially uniform increase of the d_{002}-spacing position was observed in artificially demineralised enamel, with no significant variation detected with distance from the free enamel surface to the deeper enamel. Secondly, the value of the full width at half maximum (FWHM), as related to the inverse of the crystalline length, exhibited a significant increase which was independent of the depth away from the free enamel surface [17]. Both of the aforementioned morphological discrepancies could be attributed to the different setups of the enamel sample dissolution direction (in our case, the acid was delivered from the free enamel surface into the depth towards the DEJ). This allowed monitoring the dissolution front and set up representative conditions

for investigating the consequences of the dissolution reaction. In most artificial demineralisation studies, however, the dental slices have been entirely covered in acids [17], but this would have caused difficulties in quantifying the dissolution direction and rate. It is noted that different acid types used in various studies lead to dissolving different components in the enamel [37]. It is clear nevertheless that the most significant factor controlling the demineralisation of dental enamel is the pH value (must be <4.5 [38]) and titration, whilst the acid concentration only affects the dissolution rate.

<<Fig. 9>>

Combining the observations reported, qualitative and quantitative analysis from Figures 2 to 7, a schematic representation of the observed *in situ* evolution of dental demineralisation under acid exposure is illustrated in Figure 8. Horizontally, from left to right, the diagram illustrates the structural evolution with time at a given depth from the free enamel surface, while vertically characterising the structural evolution with distance from the free enamel surface (direct acid exposure site) for a given exposure time. Each box in the diagram represents a given region in enamel within a given distance from the surface (distance is represented in the vertical axis). The red arrows indicate the direction of dissolution, SAXS total intensity (width of the arrows) and width of the SAXS total intensity peak (length of the arrows). A bundle of HAp crystallites exists in each box (depicted by the bars with different orientations). The two main morphological changes observed during demineralisation, *i.e.* crystalline length and smallest crystalline dimension, are represented by the variation in the length of the bars and the colour of the boxes. Short orange bars arose during the later demineralisation stages and represented the re-precipitation process.

In the oral environment, demineralisation and remineralisation might occur simultaneously or alternately [39]. The study presented here wasfocused on the demineralisation dynamics and the diagram provides an overview of the spatially and time-based structural changes in enamel subject to

the acid dissolution. The model may assist in understanding the mechanisms involved in the demineralisation process in enamel. Future work monitoring the complex dynamic process that involves both demineralisation and remineralisation will be explored by considering generating an artificial oral environment instead of using simple demineralising and remineralising solutions.

5. Conclusions

Advanced small angle and wide angle X-ray scattering (SAXS and WAXS) techniques have been applied to human dental enamel to characterise the *in situ* evolution of the microstructure during the chemical reaction that mimics the natural demineralisation process. The dissolution rate (5 µm/h) was estimated from the time-resolved evolution of the SAXS total intensity peak centre position. Overall, the hydroxyapatite (HAp) crystallites were dissolved as the experiment proceeded, but the heterogeneity of itsevolution was observed with a reduced smallest crystalline dimension and an enhanced degree of alignment at the free enamel surface. Such heterogeneous evolution (size, preferred orientation and degree of alignment of HAp crystallites) could be attributed to an anisotropic dissolution dependent on crystalline orientation, *i.e.* preferential rod or inter-rod demineralisation. These experiments are likely to contribute to the understanding of the caries process and assist in developing effective therapeutic treatments to promote affected dental tissues to regain structural integrity.

Acknowledgements

Author contributions

Tan Sui, Richard M. Shelton, Gabriel Landini and Alexander M. Korsunsky conceived the study. Robert Harper, Dick Shelton and Gabriel Landini prepared the samples. Tan Sui, Enrico Salvati, Robert Harper and Hongjia Zhang carried out the experiment and Tan Sui interpreted the synchrotron experimental data. Tan Sui and Alexander M. Korsunsky wrote the manuscript. All authors edited and commented on the manuscript. The authors declare that they have no competing interests.

References

[1] H.F. Chen, Y.H. Liu, Chapter 2 -- Teeth, Advanced Ceramics for Dentistry (2014) 5-21.

[2] S.F. Ang, M. Saadatmand, M.V. Swain, A. Klocke, G.A. Schneider, Comparison of mechanical behaviors of enamel rod and interrod regions in enamel, Journal of Materials Research 27(2) (2012) 448-456.

[3] A.R. Hand, M.E. Frank, Fundamentals of oral histology and physiology, Wiley Blackwell (2014).

[4] A.R. Ten Cate, A.C. Dale, Oral histology: development, structure, and function., St. Louis: Mosby (1980).

[5] E. Johansen, Comparison of the ultrastructure and chemical composition of sound and carious enamel from human permanent tooth., Tooth enamel, its composition, properties and fundamental structure. Stack M.V. and Feamhead R.W. (eds) John Wright & Sons Ltd. (1965) 177-181.

[6] S. Baron, MIcrobiology of dental decay and periodontal disease, Medical Microbiology. 4th edition, Chapter 99 (1996).

[7] C.A. Hemingway, D.M. Parker, M. Addy, M.E. Barbour, Erosion of enamel by non-carbonated soft drinks with and without toothbrushing abrasion, Br Dent J 201(7) (2006) 447-50; discussion 439; quiz 466.

[8] I.M. Low, A. Alhuthali, In-situ monitoring of dental erosion in tooth enamel when exposed to soft drinks, Mat Sci Eng C-Bio S 28(8) (2008) 1322-1325.

[9] G. Gustafson, The histopathology of caries of human dental enamel with special reference to the division of the carious lesion into zones, Acta Odontol Scand 15 (1957) 13-55.

[10] R.P. Shellis, Relationship between Human-Enamel Structure and the Formation of Caries-Like Lesions Invitro, Arch Oral Biol 29(12) (1984) 975-981.

[11] C. Robinson, J. Kirkham, R. Shore, Dental enamel: formation to destruction, Boca Raton Fla. London(CRT) (1995).

[12] M.H. van der Veen, E. de Josselin de Jong, Application of quantitative light-induced fluorescence for assessing early caries lesions, Monogr Oral Sci 17 (2000) 144-62.

[13] Z.J. Cheng, X.M. Wang, F.Z. Cui, J. Ge, J.X. Yan, The enamel softening and loss during early erosion studied by AFM, SEM and nanoindentation, Biomed Mater 4(1) (2009) 015020.

[14] M.E. Barbour, J.S. Rees, The laboratory assessment of enamel erosion: a review, J Dent 32(8) (2004) 591-602.

[15] H. Deyhle, S.N. White, O. Bunk, F. Beckmann, B. Muller, Nanostructure of carious tooth enamel lesion, Acta Biomater 10(1) (2014) 355-64.

[16] H. Deyhle, O. Bunk, B. Muller, Nanostructure of healthy and caries-affected human teeth, Nanomedicine 7(6) (2011) 694-701.

[17] S. Siddiqui, P. Anderson, M. Al-Jawad, Recovery of crystallographic texture in remineralized dental enamel, Plos One 9(10) (2014) e108879.

[18] N. Yagi, N. Ohta, T. Matsuo, T. Tanaka, Y. Terada, H. Kamasaka, K. To-O, T. Kometani, T. Kuriki, Evaluation of enamel crystallites in subsurface lesion by microbeam X-ray diffraction, J Synchrotron Radiat 16 (2009) 398-404.

[19] J. Arends, J. Christoffersen, M.R. Christoffersen, B. Ogaard, A.G. Dijkman, W.L. Jongebloed, Rate and Mechanism of Enamel Demineralization Insitu, Caries Res 26(1) (1992) 18-21.

[20] Y.M. Liao, Z.D. Feng, Z.L. Chen, In situ tracing the process of human enamel demineralization by electrochemical impedance spectroscopy (EIS), J Dent 35(5) (2007) 425-30.

[21] C. Boote, S. Dennis, R.H. Newton, H. Puri, K.M. Meek, Collagen fibrils appear more closely packed in the prepupillary cornea: optical and biomechanical implications, Invest Ophthalmol Vis Sci 44(7) (2003) 2941-8.

[22] W. Tesch, T. Vandenbos, P. Roschgr, N. Fratzl-Zelman, K. Klaushofer, W. Beertsen, P. Fratzl, Orientation of mineral crystallites and mineral density during skeletal development in mice deficient in tissue nonspecific alkaline phosphatase, J Bone Miner Res 18(1) (2003) 117-125.

[23] W. Tesch, N. Eidelman, P. Roschger, F. Goldenberg, K. Klaushofer, P. Fratzl, Graded microstructure and mechanical properties of human crown dentin, Calcified Tissue Int 69(3) (2001) 147-157.

[24] P. Fratzl, S. Schreiber, A. Boyde, Characterization of bone mineral crystals in horse radius by small-angle X-ray scattering, Calcified Tissue Int 58(5) (1996) 341-346.

[25] P. Fratzl, M. Groschner, G. Vogl, H. Plenk, J. Eschberger, N. Fratzlzelman, K. Koller, K. Klaushofer, Mineral Crystals in Calcified Tissues - a Comparative-Study by Saxs, J Bone Miner Res 7(3) (1992) 329-334.

[26] P. Fratzl, P. Roschger, J. Eschberger, B. Abendroth, K. Klaushofer, Abnormal Bone Mineralization after Fluoride Treatment in Osteoporosis - a Small-Angle X-Ray-Scattering Study, J Bone Miner Res 9(10) (1994) 1541-1549.

[27] T. Sui, M.A. Sandholzer, A.J. Lunt, N. Baimpas, A. Smith, G. Landini, A.M. Korsunsky, In situ X-ray scattering evaluation of heat-induced ultrastructural changes in dental tissues and synthetic hydroxyapatite, J R Soc Interface 11(95) (2014) 20130928.

[28] T. Sui, M.A. Sandholzer, E. Le Bourhis, N. Baimpas, G. Landini, A.M. Korsunsky, Structure-mechanical function relations at nano-scale in heat-affected human dental tissue, J Mech Behav Biomed Mater 32 (2014) 113-124.

[29] T. Sui, S. Ying, A.M. Korsunsky, G. Landini, X-ray Study of Human Dental Tissues Affected by Erythroblastosis Fetalis, J Dent Res 94(7) (2015) 1004-1010.

[30] J. Thewlis, The X-ray Examination of Enamel: (Section of Odontology), Proc R Soc Med 33(7) (1940) 387-98.

[31] F. Hirota, Prism arrangement in human cusp enamel deduced by X-ray diffraction, Arch Oral Biol 27(11) (1982) 931-7.

[32] A. Patterson, The Scherrer formula for X-ray particle size determination, Phys Rev 56 (1939) 978-982.

[33] C. Robinson, R.C. Shore, S.J. Brookes, S. Strafford, S.R. Wood, J. Kirkham, The chemistry of enamel caries, Crit Rev Oral Biol M 11(4) (2000) 481-495.

[34] S.L. Wen, Human enamel structure studied by high resolution electron microscopy, Electron Microsc Rev 2(1) (1989) 1-16.

[35] J.M. ten Cate, Remineralization of deep enamel dentine caries lesions, Aust Dent J 53(3) (2008) 281-5.

[36] E.A. Abou Neel, A. Aljabo, A. Strange, S. Ibrahim, M. Coathup, A.M. Young, L. Bozec, V. Mudera, Demineralization-remineralization dynamics in teeth and bone, Int J Nanomedicine 11 (2016) 4743-4763.

[37] R.L. Erickson, W.W. Barkmeier, N.S. Kimmes, Bond strength of self-etch adhesives to pre-etched enamel, Dent Mater 25(10) (2009) 1187-1194.

[38] P. Benjakul, C. Chuenarrom, Association of dental enamel loss with the pH and titratable acidity of beverages, J Dent Sci 6(3) (2011) 129-133.

[39] E.A. Kidd, O. Fejerskov, What constitutes dental caries? Histopathology of carious enamel and dentin related to the action of cariogenic biofilms, J Dent Res 83 Spec No C (2004) C35-8.
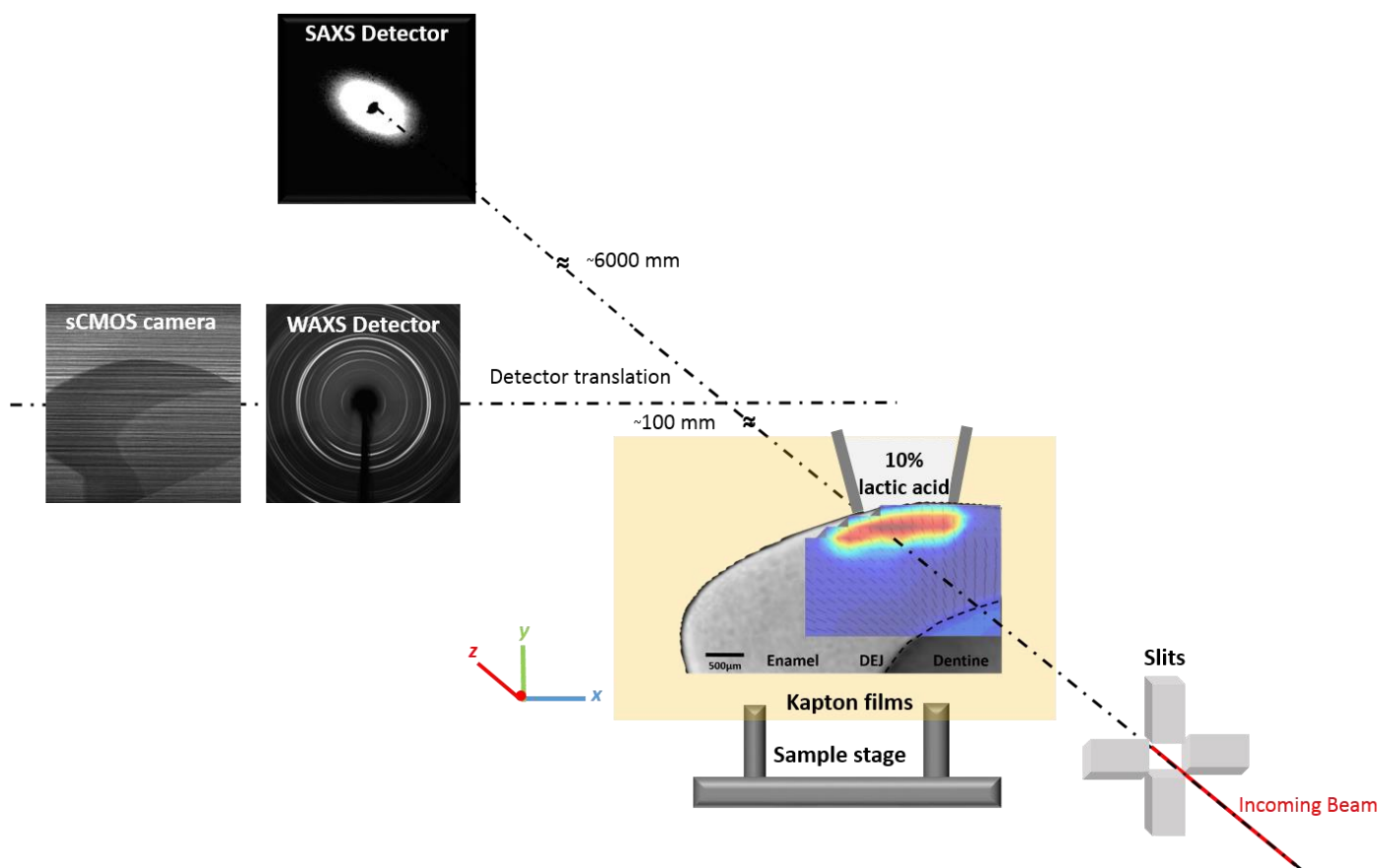
Figure captions:

Figure 1. Diagram of the *in situ* experimental set up. Two Kapton sheets were applied on the cutting surfaces of a varnished tooth slice and a funnel was made with dental ribbon wax to hold 10% v/v lactic acid, which was applied at the enamel free surface. The monochromatic X-ray beam was collimated by slits and oriented perpendicular to the sample surface. A sCMOS camera was used to ensure that the beam was illuminating the central position of enamel. WAXS diffraction patterns were recorded at each detection time. After each WAXS pattern was collected, the WAXS detector was laterally translated out of the beam to expose the SAXS detector to collect SAXS patterns.
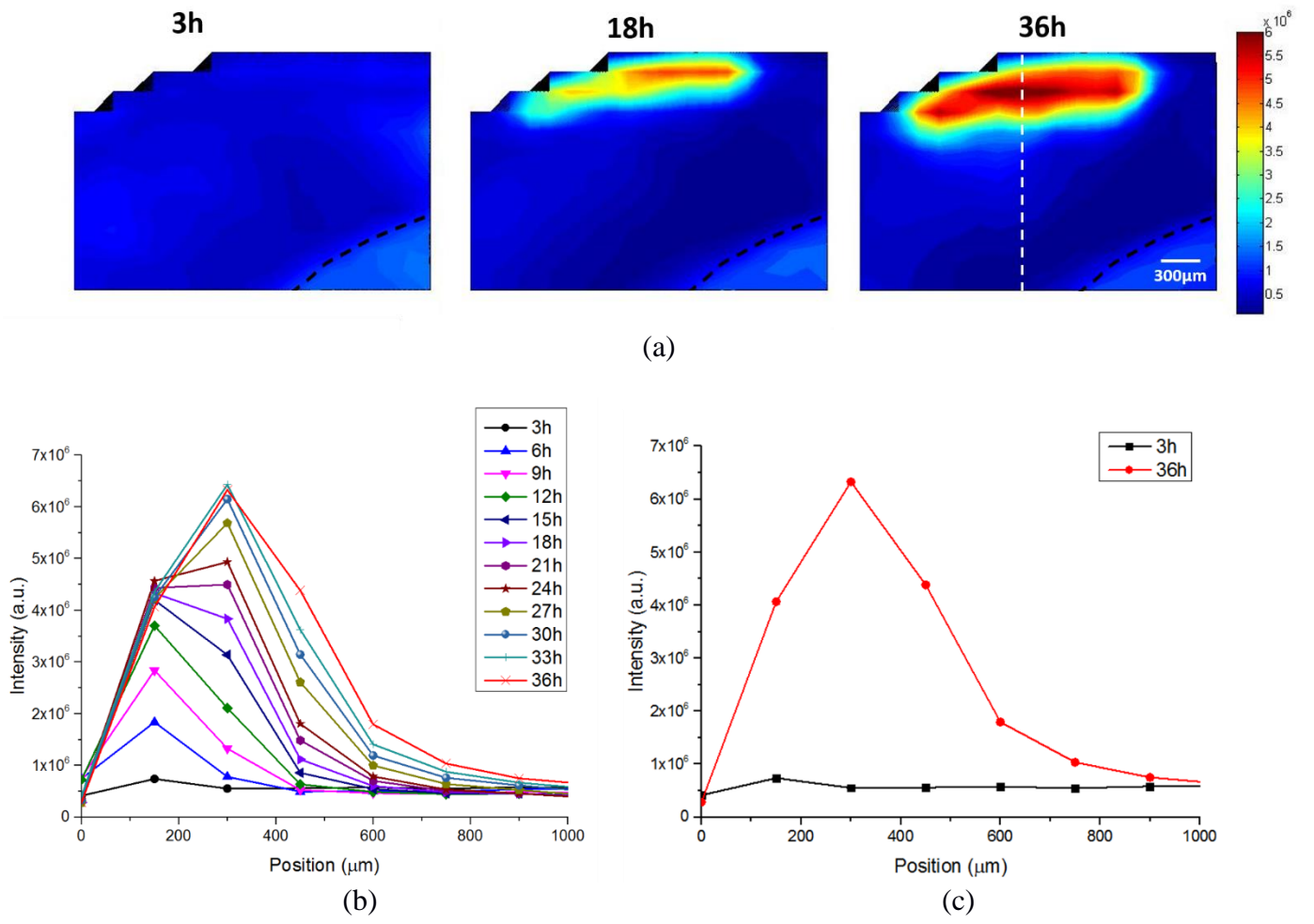
Figure 2. SAXS total intensity plots (arbitrary units). (a) Selected 2D maps at 3h, 18h and 36h (arbitrary units); Column 9 position (marked by the vertical white dashed line at 36h) is further selected for 1D profile plot; DEJ is marked by black dashed line; (b) Detailed spatial 1D evolution of the intensity with time period from 3h to 36h; (c) Comparison of the 1D profiles at early stage (3h) and later stage (36h).
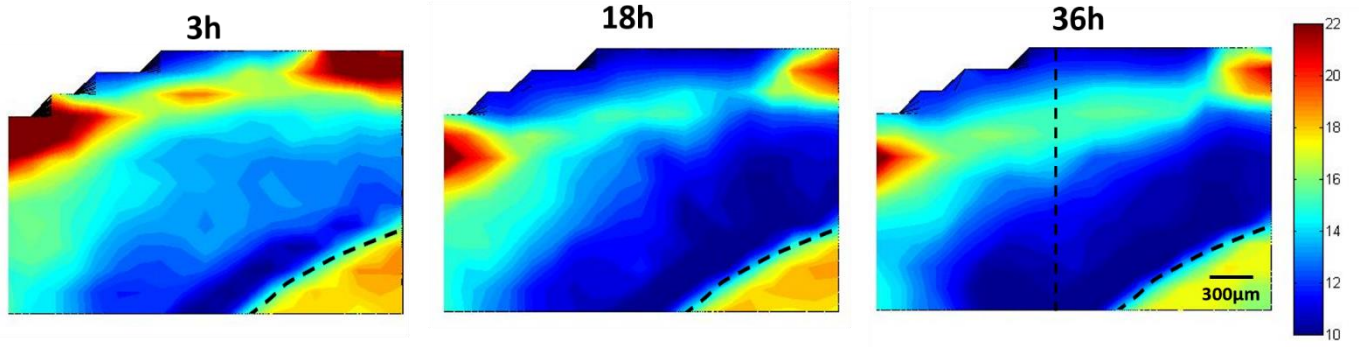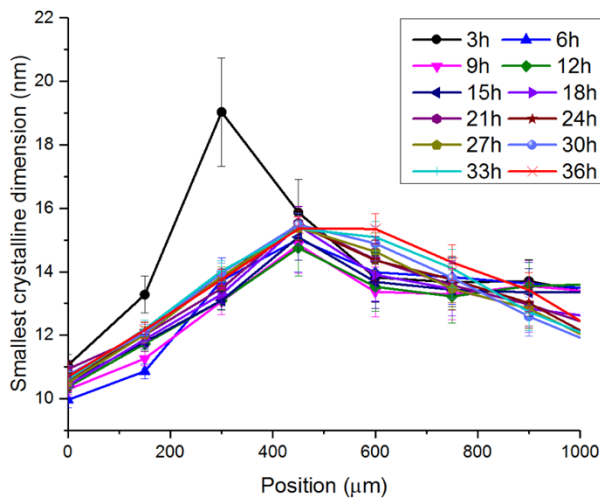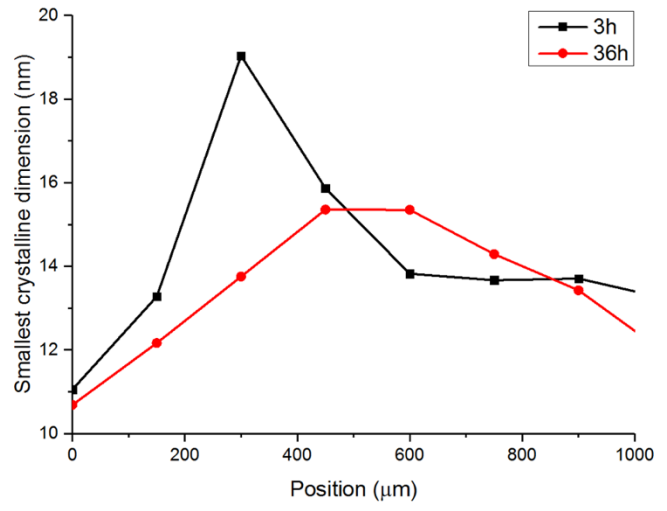
Figure 3. SAXS smallest crystalline dimension plots (unit: nm). (a) Selected 2D maps at 3h, 18h and 36h (unit: nm); the black dashed line at 36h marks the same position as shown in Figure 3b for quantitative 1D profile plot; DEJ is marked by black dashed line; (b) Detailed spatial 1D evolution of smallest crystalline dimension with time period from 3h to 36h; (c) Comparison of the 1D profiles at early stage (3h) and later stage (36h).
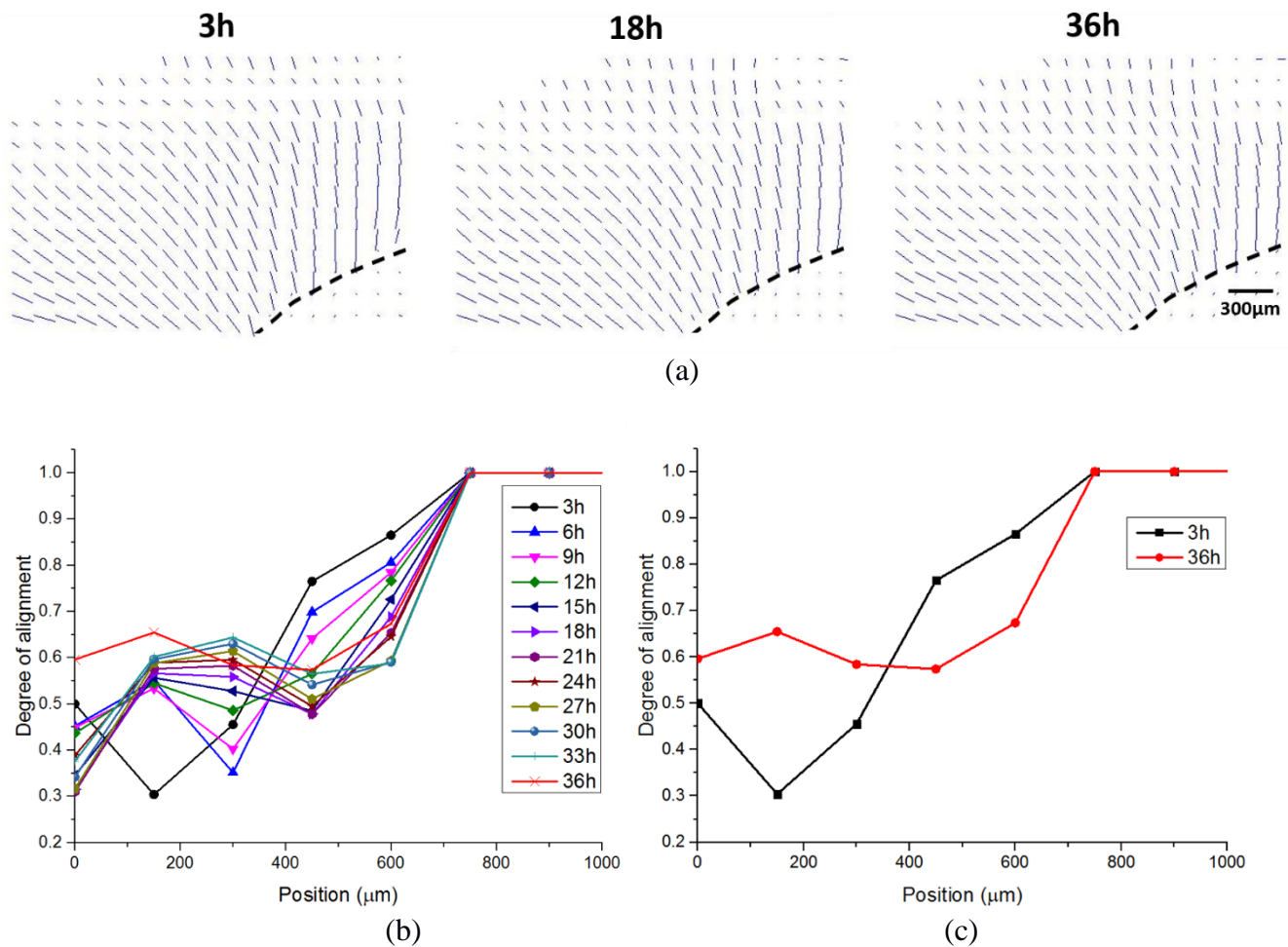
Figure 4. SAXS crystalline preferred orientation and degree of alignment plots. (a) Selected 2D maps at 0h, 3h, 6h, 12h, 18h and 36h; the bar orientation at each position is the preferred orientation while the length of the bar represents degree of alignment. DEJ is marked by black dashed line. There are visible changes of the preferred orientation and degree of alignment in the central region of the diagrams with time varying between the 3h, 6h and 18h. Column 9 was chosen to generate 1D profile plots; (b) Detailed 1D representation of the spatial variation of degree of alignment with time from 3h to 36h. (c) Comparison of the 1D profiles between an early stage (3h) and a later stage (36h).
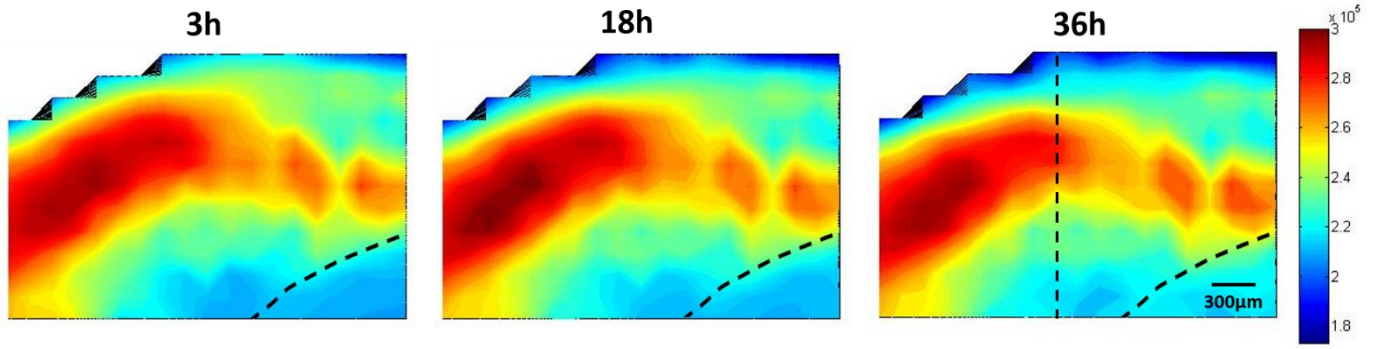
(a)
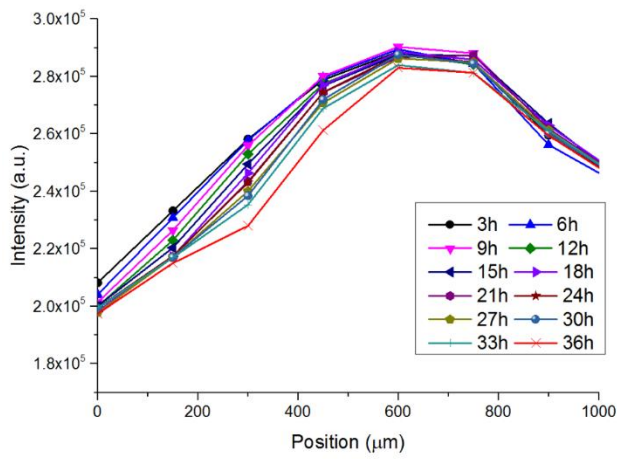
(b)
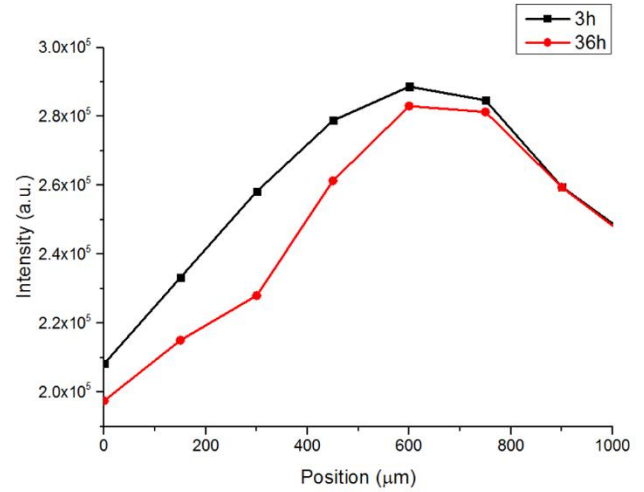
(c)

Figure 5. WAXS (002) peak intensity plots (arbitrary units). (a) Selected 2D maps at 3h, 18h and 36h (unit: a.u.); the black dashed line at 36h marks the position for 1D profile plot; DEJ is marked by black dashed line; (b) Detailed spatial 1D evolution of intensity with time from 3h to 36h; (c) Comparison of the 1D profiles at early stage (3h) and later stage (36h).
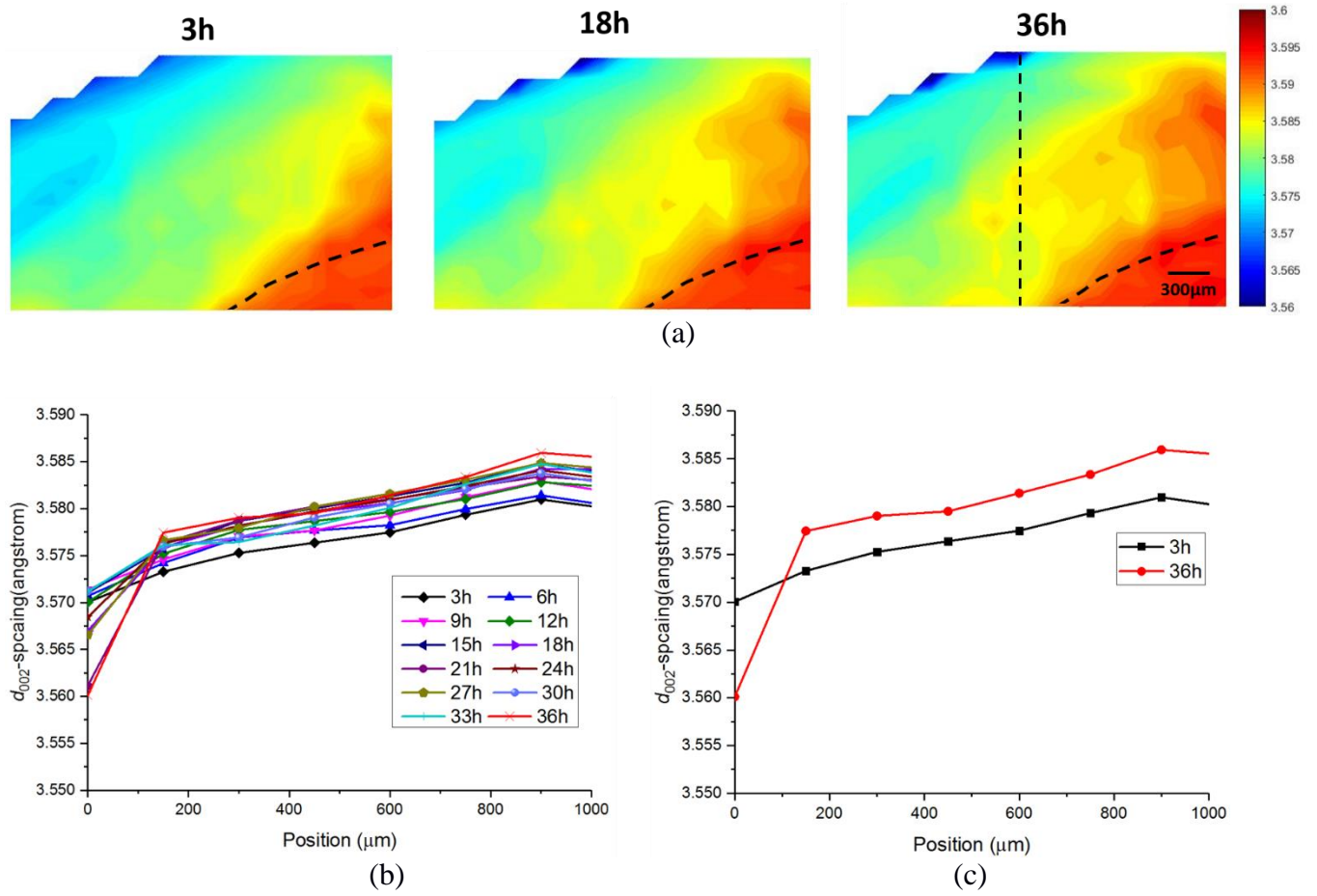
Figure 6. WAXS d_{002}-spacing plots (unit: Ångstrom). (a) Selected 2D maps at 3h, 18h and 36h (unit: angstrom); the black dashed line at 36h marks the position for 1D profile plot; DEJ is marked by black dashed line; (b) Detailed spatial 1D evolution of d_{002}-spacing with time from 3h to 36h (error<1E-03); (c) Comparison of the 1D profiles at early stage (3h) and later stage (36h).
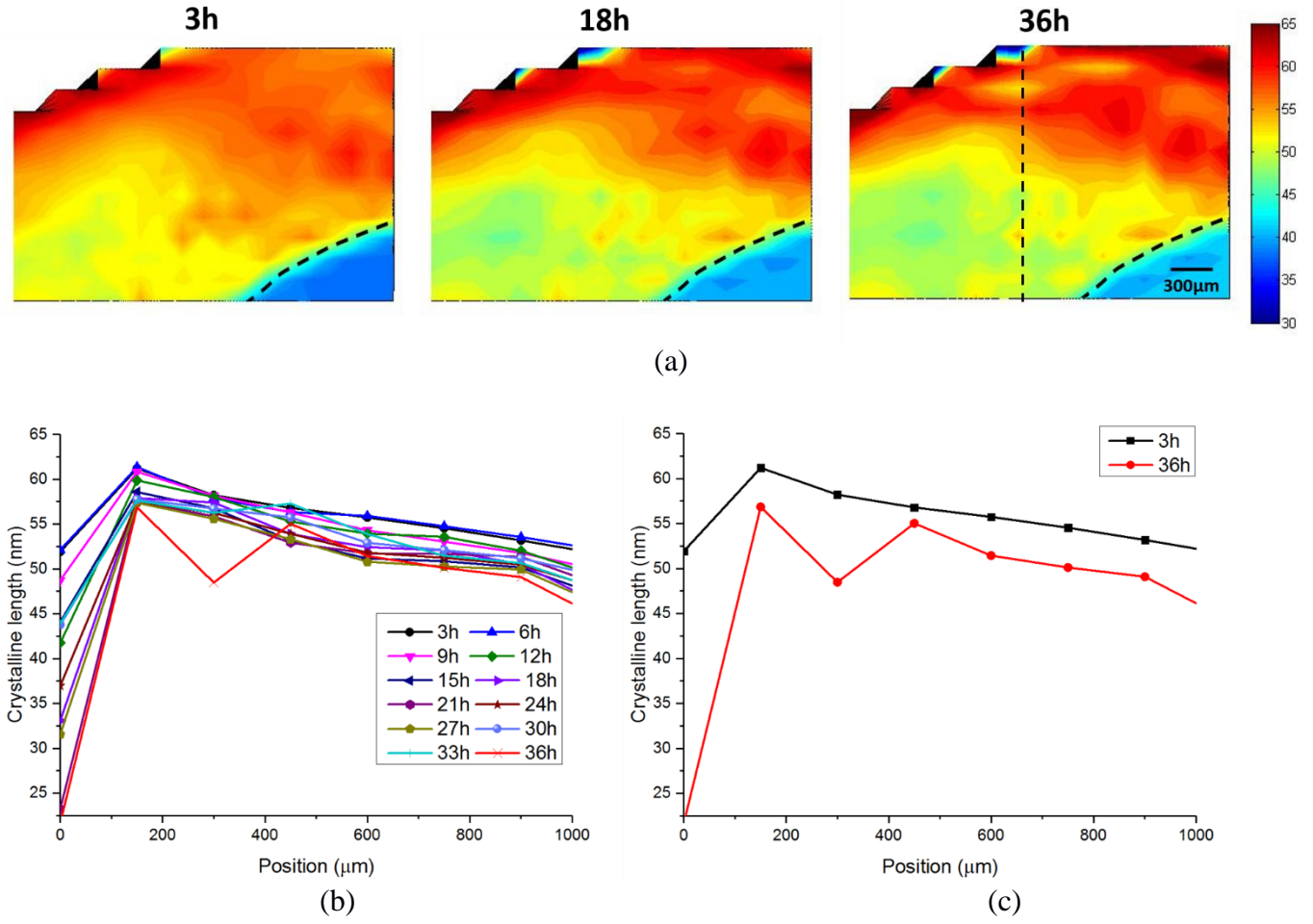
Figure 7. WAXS crystalline length plots (unit: nm). (a) Selected 2D maps at 3h, 18h and 36h (unit: nm); the black dashed line at 36h marks the position for 1D profile plot; DEJ is marked by black dashed line; (b) Detailed spatial 1D evolution of crystalline length with time from 3h to 36h (error<5E-2nm); (c) Comparison of the 1D profiles at early stage (3h) and later stage (36h).
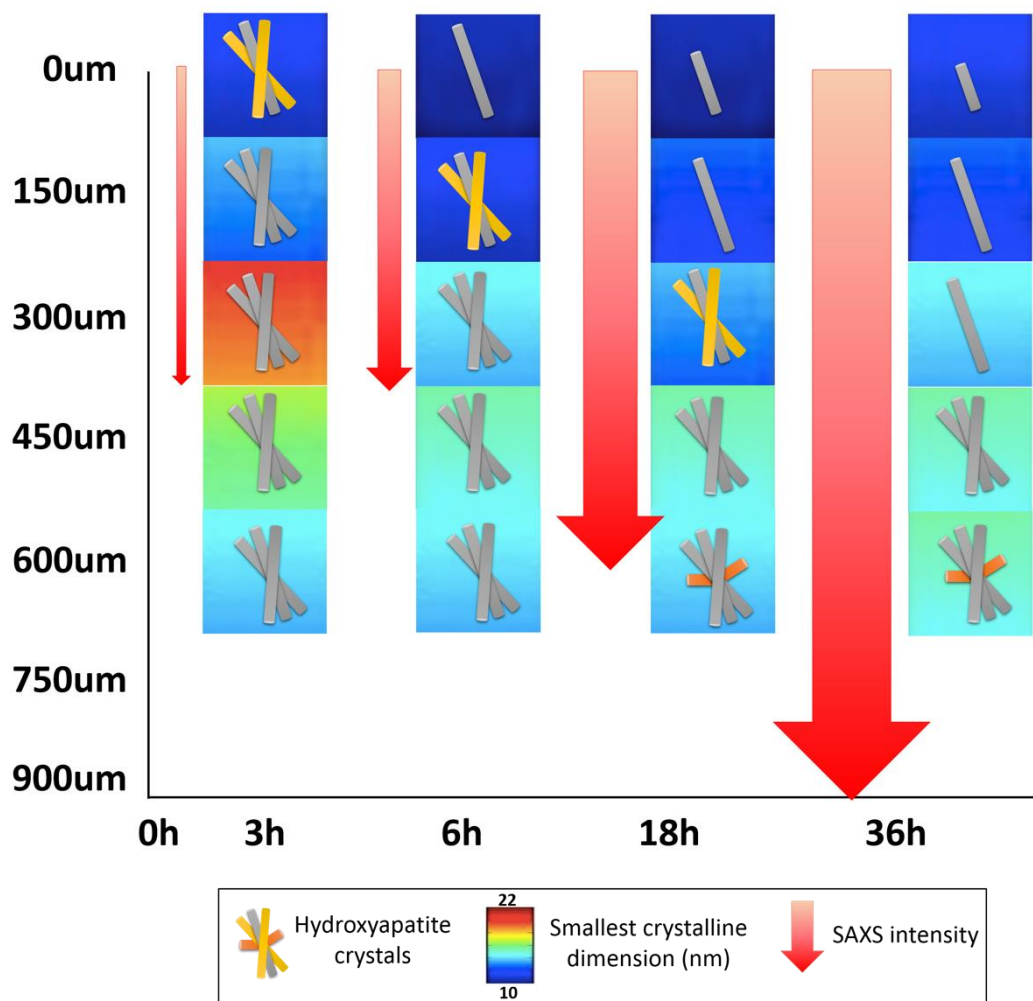
Figure 8. Schematic illustration of the correlation between the time-resolved evolution process of HAp crystallites demineralisation and the collected SAXS/WAXS information of the dental enamel subject to acid exposure. The red arrow has three features: the direction depicts the dissolution direction; the width represents the magnitude of SAXS total intensity (see Figure 2); the length shows the width of the SAXS total intensity peak (Figure 2). The colour bar of the boxes represents the smallest crystalline dimension measured by SAXS (see Figure 3). The bars in each box represent the HAp crystallites, with the geometric features of length obtained by WAXS (see Figure 7) and preferred orientation obtained by SAXS (see Figure 4). Bars with other orientations are added to reflect the degree of alignment (Figure 4), with the ones marked in yellow depicting the crystallites to be dissolved at the next stage. The short orange bars appeared at 400 µm enamel depth dictates the re-precipitation on HAp crystallites.